Focused Ion Beam Induced Nanojunction and Defect Doping as a Building Block for Nanoscale Electronics in GaN Nanowires

S. Dhara,*,†,§ C. Y. Lu,† C. T. Wu,‡ C. W. Hsu,‡ W. S. Tu,† K. H. Chen,*,† Y. L. Wang,† L. C. Chen,‡ and Baldev Raj§

Institute of Atomic and Molecular Sciences, Academia Sinica, Taipei 106, Taiwan, Center for Condensed Matter Science, National Taiwan University, Taipei 106, Taiwan, and Surface and Nanoscience Division, Indira Gandhi Centre for Atomic Research, Kalpakkam-603102, India

Received: March 8, 2010; Revised Manuscript Received: July 13, 2010

Two GaN nanowires are formed as a nanojunction using focused ion beam (FIB) assisted implantation of Ga^+ self-ion. FIB-induced metallization and electrical isolation by cutting the nanowires are also used for the completion of contact formation. Defect doping, employing the formation energies of vacancies and interstitials, in the energetic nonequilibrium ion beam processing is successfully attempted for the formation of a *p*-type GaN nanowire. Detailed transport measurements of welded nanojunctions and rectification in the form of *p*−*n* junctions for two nanowires are reported in this process of in situ nanoengineering. The rectification is also reported for the *p*−*n* junction formed in a single nanowire. This is a unique technique demonstrating an all FIB nanoelectronic fabrications for future miniaturization of devices.

Introduction

There is an impetus for the formation of nanojunctions (NJs) as building block nanoelectronics. Rectification is demonstrated in NJs formed by crossing single-walled metallic carbon nanotubes (SWCNT) with semiconducting ones,[1] in *p*- and *n*-type elemental Si,[2] compound GaN,[3,4] and InP[5] semiconductor nanowires (NWs) crossed with their respective *n*-type counterparts and in “heterojunctions” created either by crossing a *p*-type Si NW, with an *n*-GaN NW.[6,7] Physical contacts are evidenced for the formation of *p*−*n* junctions and many of the reports find it as a statistical event. A *p*−*n* junction is also reported in a single piece-wise-doped silicon NW produced by modulation doping, which is an expensive and time-consuming, but more accurate, technique.[8] One of the aims of nanoscience and technology is to create low-dimensional structures with electronic properties that replicate those of the conventionally fabricated systems. However, it is difficult to do so in ultrasmall structures created by alternative synthetic means. Over years, metallization or gate oxidation processes for nanostructures are standardized by various well-established techniques, namely, electron beam lithography or focused ion beam or electron beam assisted metal/insulator deposition techniques. An ultrasonic welding for metallization and its electrical transport properties are also reported of SWCNT.[9] Y-junction SWCNT is reported to form new heterojunctions for the nanoelectronics.[10] Leaving synthetic routes for the formation of “Y” junctions in CNTs,[10,11] an electron beam welding of two SWCNT[12] is one of the novel approaches for engineering the NJ formation. Except for a possible alternative to chemical functionalization, however, no electrical transport properties demonstrating the physical state of contact formation are reported in these electron-beam welded nanostructures.

* To whom correspondence should be addressed. E-mail: dhara@igcar.gov.in; chenkh@pub.iams.sinica.edu.tw.
† Academia Sinica.
§ Indira Gandhi Centre for Atomic Research.
‡ National Taiwan University.

In this presentation, we report nanoengineering for electronics comprising of electrical isolation, metallization, junction formation and doping of GaN NWs using focused ion beam (FIB). Electric and photoelectric transport properties of few representative configurations are also reported. Ion beam assisted disintegration of trimethyl cyclopentadienyl platinum ($C_9H_{16}Pt$) is used for the metallization purpose. At optimal fluences, FIB-assisted Ga^+ is used for the electrical contact formation in the process of nanowelding of GaN NWs as a self-ion weld-mate. Energetic Ga^+ FIB with high fluences are used for isolation of NW(s) for the purpose of studying a specific configuration of NW (elimination of unwanted portions). Nanowelding is used for the formation of NJs of two separate NWs. Nominal *p*-type doping in one of the welded NWs and in one-half of the same NW are performed using ion beam assisted engineering of native defects in the GaN NW. While metallization, electrical isolation and nanowelding provide control for the formation of NJs, deployment of native defects for useful *p*-type doping is unique in the present study.

Experimental Details

GaN NWs grown on Si (100) substrate by catalyst-assisted vapor−liquid−solid (VLS) mechanism were used for this study.[13] In the VLS process, Au nanoclusters are used as a catalyst and for the growth of wurtize GaN NWs with growth direction along [110].[14] These NWs were intrinsically *n*-type.[15] They were physically transferred (gentle mechanical tapping on the back of the grown substrate, while the collecting substrate was placed below) to patterned substrate with Au as metal contact pads and SiN_x as an insulating layer. It is shown in the scanning electron microscopic (SEM) image (Figure 1a). A dual beam focused ion beam system (FEI NOVA-600) with a SEM and a 30 KeV Ga^+ FIB at varying fluences were used for metallization (1E10 ions$\cdot$cm^{-2}) in NWs with different configurations (Figure 1b,c), isolation of NW(s) using fluence of 1E18 ions$\cdot$cm^{-2} (Figure 1c,d), nanowelding in the fluence range of 4E15−6E15 ions$\cdot$cm^{-2} of two NWs (Figure 1c) and doping with fluences of 7E14, 1E15, and 2E15 ions$\cdot$cm^{-2} with ion flux

10.1021/jp1020998 © 2010 American Chemical Society
Published on Web 08/23/2010

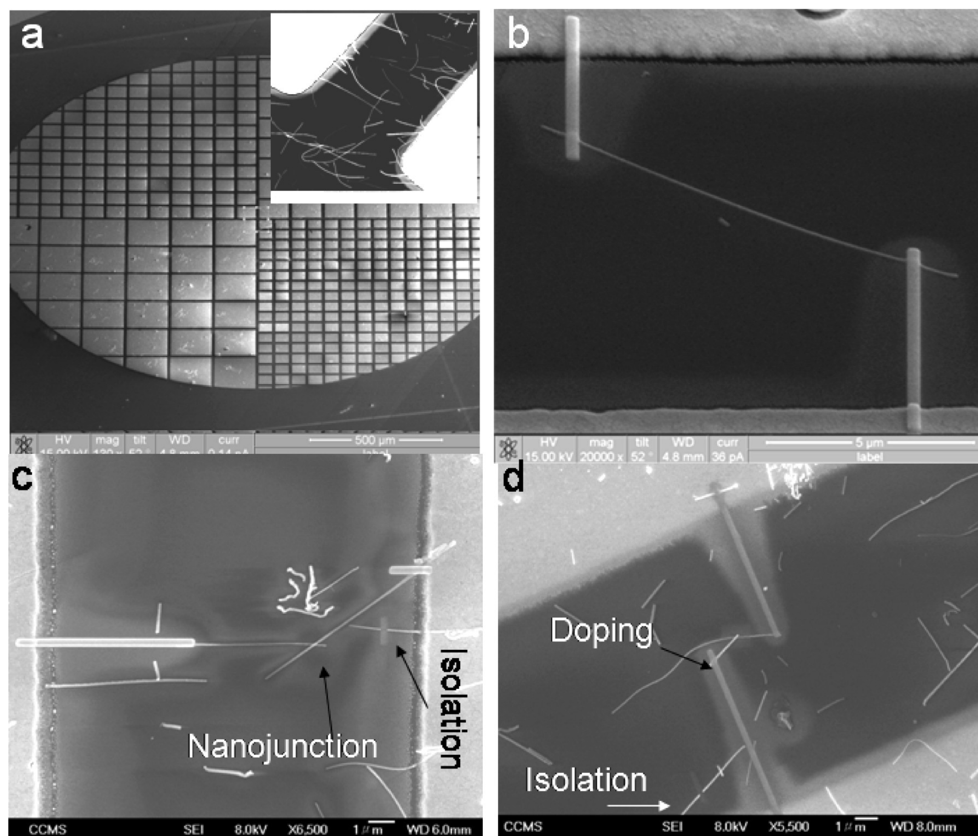

Figure 1. Typical configurations and features of (a) dispersion of nanowires with a close view in the inset (in situ FESEM image of FIB), metallization of (b) a single nanowire (in situ FESEM image of FIB) and (c) two nanowires with welded nanojunction (ex situ image with JEOL FESEM), and (d) defect doping in one of the nanowires, as indicated. Isolation of unwanted nanowires is typically shown in both (c) and (d).

below 5×10^{12} ions·cm^{-2}·sec^{-1} for a typical NW (Figure 1d). Field emission SEM (FESEM, Model JEOL JSM-6700F) was used for ex situ snaps of the contacts. The FIB system was also equipped with a pair of microprobes (Kleindiek) for in situ electrical transport measurements. Depending on the physical configuration of different junctions the nanowelded area was varied with the objective of minimum area exposed to Ga^+ beam outside the junction area. The samples were annealed in ultra high pure (UHP) N_2 atmosphere at 973 K for 2 min. Metallization was checked in situ, showing Ohmic conduction in the electrical transport measurements at room temperature (RT) for a single NW connected by FIB with the Au contact pad before and after annealing. Current value close to one order higher in magnitude was recorded in the annealed samples (please see Supporting Information, Figure S1).

In our previous reports on detailed self (Ga^+)-ion implantation studies in GaN NWs, we have understood the behavior of formation and annealing of point defects,[14,16] role of defects is nucleation of a second phase as a typical case of solid−solid phase transition,[17] details of amorphization and beyond, as well as the mechanism for blister formation.[18] In our studies and in the reports by other researchers thereafter,[19,20] it is well established that a dynamic annealing (defect annihilation) takes place by monoenergetic FIB implantation on GaN NWs and it is effective only at an optimum fluence. In general, the annihilation of defects by the dynamic annealing process at low fluences is less efficient and the efficiency goes better with increasing fluence. However, a competitive process of point-defect cluster formation comprised of mainly complexes of vacancies and interstitials with a further increase of ion fluence leads the total process of dynamic annealing to be inefficient again. An additional increase in the fluence amorphizes the surface layer completely. Accumulation of defect-clusters at high fluences forces the dynamic annealing to be inefficient and, thus, a large scale amorphization is observed. We set optimal fluences for nanowelding close to 5E15 ions·cm^{-2},[14] which is also the value reported for phase transitions in GaN NWs under self-ion implantation.[17]

Results and Discussion

Electrical Contact Formation and Nanowelding. We have studied electrical transport measurements both in situ (at a pressure $\sim 1 \times 10^{-5}$ mbar) and ex situ (at RT and atmospheric pressure, RTP) to confirm the minimum fluence required for the connectivity (Figure 2a−c) of two nanowelded NWs. A typical in situ pressure contact is shown along with the FESEM image of the contacts (Figure 2a). In situ two-probe electrical transport measurements (Figure 2b) were performed with accumulating fluences. The study showed a proper Ohmic plot with a net nanowelding fluence of 6E15 ions·cm^{-2}. In case of ex situ electrical transport measurements (Figure 2c) at RTP, however, a reasonable connectivity was recorded for a fluence of 4E15 ions·cm^{-2} onward and the trend was compared with a single NW connected by FIB-assisted metallization (Figure S1). We must state here that we studied different welding fluences for different sets of NWs in the RTP measurements (corresponding FESEM images of contacts for NJs are shown in the inset of Figure 2c), as we have optimized the fluence for junction formation in the same exposure of the FIB chamber, avoiding multiple exposure of the NW sets to air. So the current values are not really comparable to each other. The samples are also not annealed in RTP measurements for the sake of comparison with the in situ measurements. Inference on junction formation should not differ, however, whether the measurement is

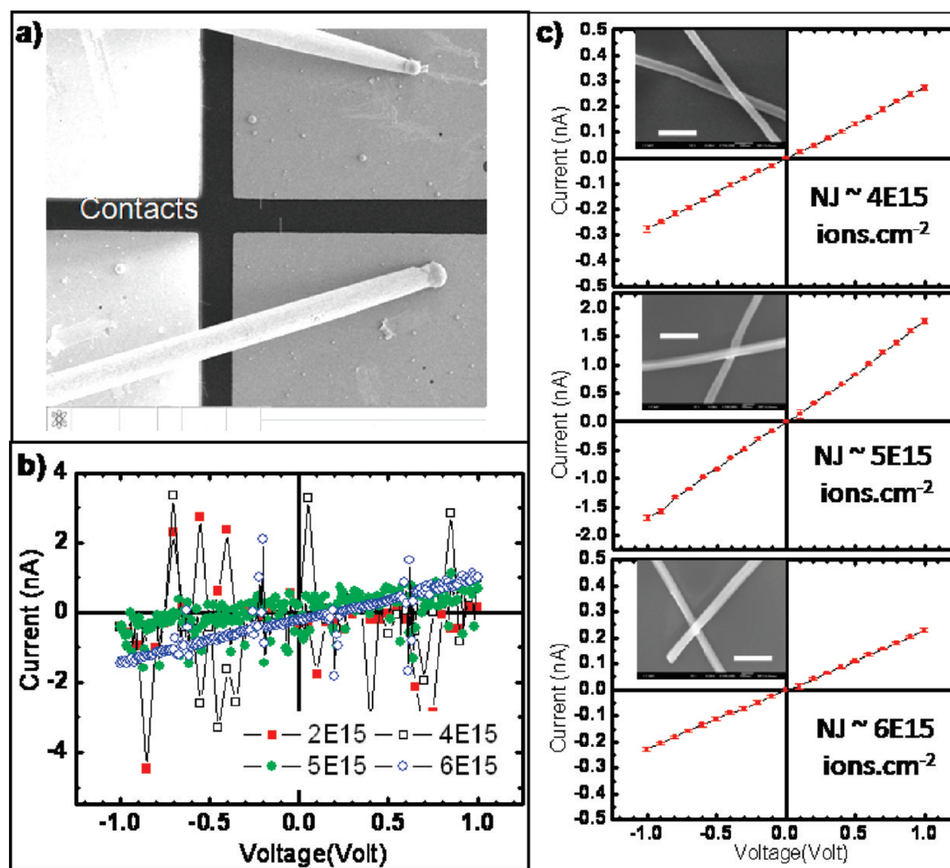

Figure 2. Ascertaining electrical connectivity via Ohmic contact formation. (a) Image (FIB FESEM) of typical two-probe measurements indicating contacts of NW in the actual measurement; (b) in situ measurements for the nanojunctions (NJs) formed with incremental fluences up to 6E15 ions·cm^{-2}; and (c) ex situ measurements for the NJs formed at various fluences as inscribed. JEOL FESEM images of the respective NJs are shown in the insets. Scale bars are 300 nm.

performed in situ or ex situ. Thus, while choosing 4E15 ions·cm^{-2} as a proper fluence for the NJ formation, the trend of Ohmic conduction is only considered. In further resolving differences in the Ohmic contact observed in the in situ and ex situ electrical transport measurements, we must state that the conditions in vacuum and at RTP are never same, particularly, in quantitative measurements for various issues related to ambient at pressure-contact region and contributions from accumulated charges in the sample originating during FIB or SEM scanning. In case of in situ measurements, we have minimized the charge accumulation effect by proper contact of the substrate to the ground, in general, and using a minimum SEM and FIB scan. As a matter of fact, the charge accumulation effect was so strong that during our trial measurements the Au contact pad exploded under the tungsten probe during progressive fluences, and at that time the probe itself got slashed (Supporting Information, Figure S2). We restricted our measurements for the NWs nanowelded with fluence of 5E15 ions·cm^{-2} or below.

The FESEM images along with corresponding field emission scanning tunneling electron microscopy (STEM, FEI Tecnai F20 200 kV with high resolution <0.2 nm) based high angle annular dark field (HAADF) images (Figure 3a) are shown for the NJs formed by Ga^+ fluences of 4E15 and 5E15 ions·cm^{-2}. Electron energy loss spectra (Figure 3b) are shown for corresponding points marked in HAADF images. Plasmon peaks at 19.6 eV in the unwelded NW junction correspond to GaN bulk plasmon. A new peak at 14 eV, corresponding to Ga plasmon, was found in the junction region of the welded NWs. Presence of GaN bulk plasmon was also observed at the edge of the NJs. Plasmon imaging (Figure 3c) using energy window corresponding to 14 eV showed the presence of elemental Ga at the NJ to promote nanowelding and activate Ohmic conductivity for both the fluences. Plasmon imaging (Figure 3c) with energy window corresponding to 19.6 eV showed that the welded NWs were predominantly GaN. A minor defect, observed in one of the NWs is in the pristine sample, is not an effect of ion implantation as there is no trace of Ga in the EELS spectra close to the defect region. The peak observed at 24 eV correspond to amorphous C of the TEM grid.[21]

As compared to that for single NW (Figure 4a), a nanowelded postannealed junction was further qualified with photoconductivity (PC) measurements (Figure 4b) with the exposure of He–Cd laser (325 nm). With the reported band gap of 3.46 eV in the GaN a PC would be generated with the excitation of 325 nm (~3.81 eV). Persistent photocurrent measurements in the nanowelded NWs also showed fairly comparable decay constant of ~2000 s and a decay exponent ~0.3, as compared to corresponding reported[22] values of ~544 s and 0.46 for *n*-GaN film showing no major defect states in the nanowelding process (Figure 4c).

Defect Doping in the Nanowires. In an attempt to dope one of the NW, we have resorted to creation of native defects in GaN NW using energetic Ga^+ implantation. Molecular dynamics based ab initio calculations using supercell technique predicted formation of deep acceptor states by Ga vacancy (V_{Ga}), Ga interstitial (Ga_I) and N antisites (N_{Ga}), and V_N forming shallow donor states.[23] Formation energies for these defect states[24] can be provided in the energetic process adopted in this report. A large amount of V_{Ga} was produced with maximum energy being

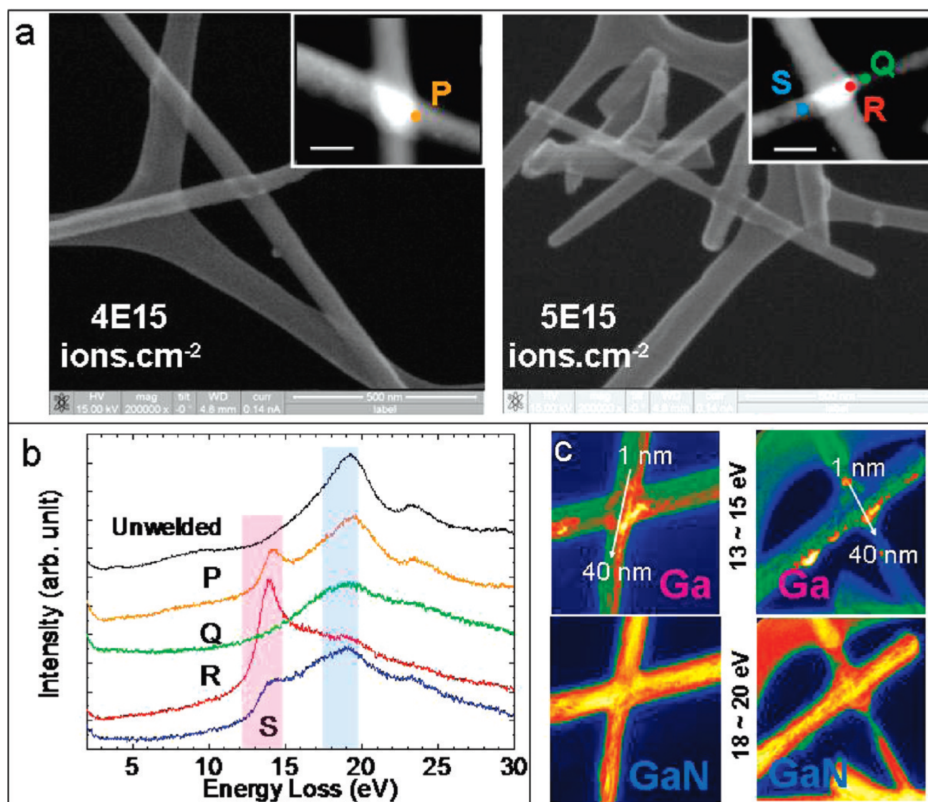

Figure 3. Electronic qualification of the nanojunctions (NJs). (a) FIB FESEM and corresponding STEM-assisted HAADF images NJs formed by different fluences as inscribed. Scale bar is 50 nm. (b) Electron energy loss spectra (EELS) for the unwelded NJs and different spots of welded NJs shows presence of Ga in the welded region; (c) plasmon imaging with the use of energy windows corresponding to elemental Ga and bulk GaN showing the location of Ga accumulation. The NWs shown in (a) and (c) are the same, but images are not shown for the same orientation.

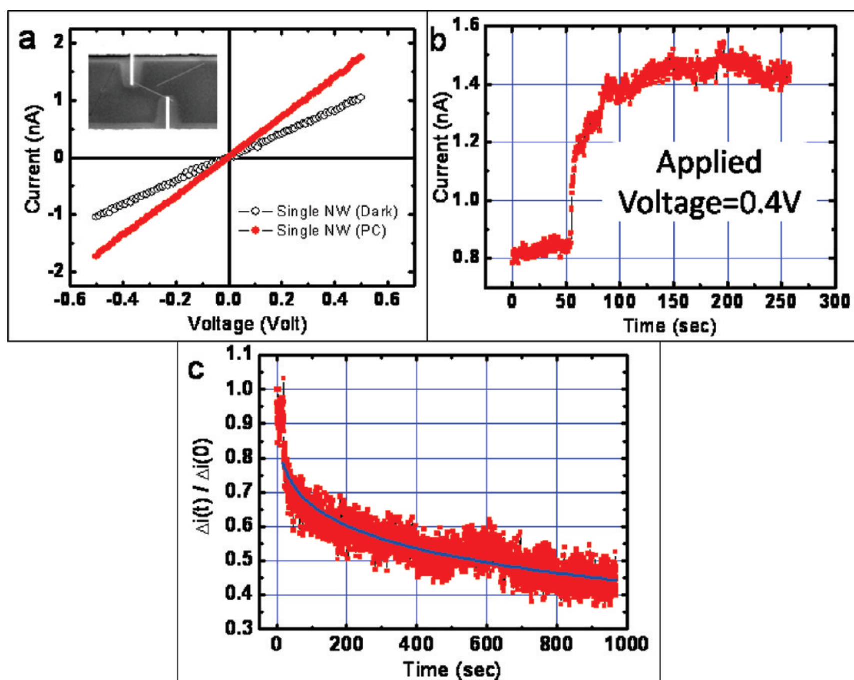

Figure 4. Photoconductivity (PC) measurements in (a) $I-V$ characterization of a single NW in the dark condition and 325 nm laser exposure. (b) Time-dependent PC measurements in a nanowelded nanowire system typically formed with a fluence of 5E15 ions$\cdot$cm^{-2} measure at an applied voltage of 0.4 V. (c) Persistent PC for the same nanowelded nanowires.

transferred (E) on target (M_T) Ga atoms in the head-on collision of equal masses in the projectile (M_P) energy of the projectile E_0) and target; $E = E_0((4M_PM_T)/((M_P + M_T)^2))$. However, in the presence of excess Ga in the self-ion implanted sample, annealing treatment in the UHP N_2 ambient was anticipated to compensate for at least a few of the V_{Ga} and leaving some amount of N_{Ga} present in the system. Considering the nonequilibrium process of ion implantation, we have implanted Ga^+ for the fluences of 7E14, 1E15, and 2E15 ions$\cdot$cm^{-2} to have a control in the defect production. A rectification behavior in the

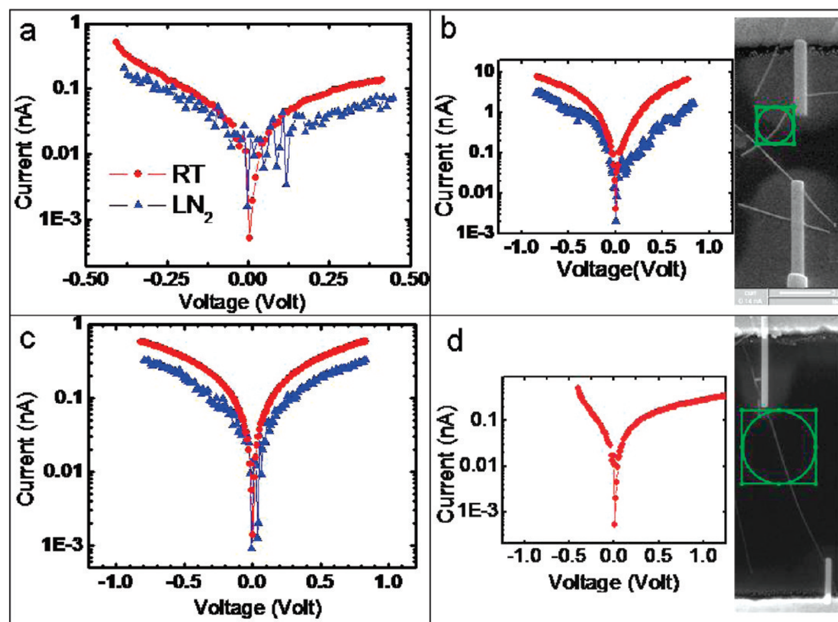

Figure 5. Rectification at different temperatures (RT ∼ 300 K and LN_2 ∼ 77 K) in the nanowelded nanowire systems formed with fluences of (a) 7E14 ions·cm^{-2}; (b) 1E15 ions·cm^{-2}, along with an image of the doped junction, as marked, and (c) 2E15 ions·cm^{-2}. (d) Rectification at RT is shown for a single GaN nanowire along with an image of the NW doped for one-half, as marked.

current voltage ($I-V$) characteristic at RT is shown only for the postannealed sample implanted with a fluence of 7E14 ions·cm^{-2}. We assign N_{Ga} for the p-type doping with expected acceptor level E_v + 0.4 eV in the RT measurements (Figure 5a). We must restate here that the pristine GaN NWs are intrinsically n-type. V_N with shallow donor level is primarily responsible for the n-type conductivity. Absence of a clear rectification at RT in the sample implanted with fluences above 1E15 ions·cm^{-2} might be due to lack of p-type doping in these samples (Figure 5b,c). Typical image of the $p-n$ junction, doped at 1E15 ions·cm^{-2} of Ga^+ is shown in the outset of Figure 5b. The disappearance of rectification behavior may be explained based on our postulation of lack of N_{Ga} in these samples. The deficiency might be due to the fact that dynamic annealing of V_{Ga} site with increasing Ga^+ fluence left little chance for the formation of N_{Ga} in the subsequent annealing process. Nevertheless, for p-type doping, an alternative possibility was Ga_I with acceptor levels of E_v + 1.7 eV (ideal, O) and E_v + 0.7 eV (relaxed, T) for different atomic configurations of interstitial site. High mobility of interstitial was unlikely to show any doping effect in the RT measurements. However, minor rectification was shown in $I-V$ characteristic of all the samples (Figure 5a−c) when measured at liquid nitrogen temperature (77 K). Thus, a contribution from the Ga_I at low temperature for p-type doping in nanowelded GaN NWs could not be overlooked. Excess presence of Ga may result in the pile up of electrostatic charge at the nanowire junction. Interference of electrostatic field at the junction may alter the injection of carries leading to diminished amount of rectification,[25] as observed in the case of nanowelded junctions. As a matter of fact, our study with a single GaN NW exposed one-half with a fluence of 1E15 ions·cm^{-2} showed excellent rectification property at RT (Figure 5d). The rectification was prominent in the absence of junction.

Conclusions

With few representative examples, we show the capability of FIB as a tool for engineering nanoelectronics, which may be useful in future down-scaling of integrated circuits. We use nanoscale metallization of nanostructures to macroscopic contact pad by ion beam assisted deposition of organometallic precursor, isolation of nanostructures using ion beam at high fluence, nanowelding of nanostructures for the formation of nanojunctions, and finally doping of semiconducting nanowire using native defects formed in the ion implantation and subsequent annealing processes.

Acknowledgment. Technical support from P. C. Kuo and J. Shiue at NanoCore, the Core Facilities for Nanoscience and Nanotechnology at Academia Sinica, Taipei, Taiwan, is acknowledged. We also thank National Science Council, Taiwan for the research grant.

Supporting Information Available: Additional supporting figures. This material is available free of charge via the Internet at http://pubs.acs.org.

References and Notes

(1) Fuhrer, M. S.; Nygard, J.; Shih, L.; Forero, M.; Yoon, Y.-G.; Mazzoni, M. S. C.; Choi, H. J.; Ihm, J.; Louie, S. G.; Zettl, A.; McEuen, P. L. *Science* **2000**, *288*, 494–497.

(2) Cui, Y.; Lieber, C. M. *Science* **2000**, *291*, 891–893.

(3) Zhong, Z.; Qian, F.; Wang, D.; Lieber, C. M. *Nano Lett.* **2003**, *3*, 343–346.

(4) (a) Cheng, G.; Kolmakov, A.; Zhang, Y. X.; Munden, R.; Reed, M.; Wang, G.; Moses, D.; Zhang, J. P. *Appl. Phys. Lett.* **2003**, *83*, 1578–1580. (b) Kim, J.-R.; Oh, H.; So, H. M.; Kim, J.-J.; Kim, J.; Lee, C. J.; Lyu, S. C. *Nanotechnology* **2002**, *13*, 701–704.

(5) Duan, X.; Huang, Y.; Cui, Y.; Wang, J.; Lieber, C. M. *Nature* **2001**, *409*, 66–69.

(6) Yu, H.; Duan, X.; Cui, Y.; Lieber, C. M. *Nano Lett.* **2002**, *2*, 101–104.

(7) Yu, H.; Duan, X.; Cui, Y.; Lauhon, L. J.; Kim, K.-H.; Lieber, C. M. *Science* **2001**, *294*, 1313–1317.

(8) Gudiksen, M. S.; Lauhon, L. J.; Wang, J.; Smith, D.; Lieber, C. M. *Nature* **2002**, *415*, 617–620.

(9) Chen, C.; Yan, L.; Kong, E. S.-W.; Zhang, Y. *Nanotechnology* **2006**, *17*, 2192–2197.

(10) Papadopoulos, C.; Rakitin, A.; Li, J.; Vedeneev, A. S.; Xu, J. M. *Phys. Rev. Lett.* **2000**, *85*, 3476–3479.

(11) Gan, B.; Ahn, J.; Zhang, Q.; Rusli Yoon, S. F.; Yu, J.; Huang, Q.-F.; Chew, K.; Ligatchev, V. A.; Zhang, X.-B.; Li, W.-Z. *Chem. Phys. Lett.* **2001**, *333*, 23–28.

(12) Terrones, M.; Banhart, F.; Grobert, N.; Charlier, J.-C.; Terrones, H.; Ajayan, P. M. *Phys. Rev. Lett.* **2002**, *89*, 075505−1-4.

(13) Chen, C. C.; Yeh, C.-C.; Chen, C.-H.; Yu, M.-Y.; Liu, H.-L.; Wu, J.-J.; Chen, K.-H.; Chen, L.-C.; Peng, J.-Y.; Chen, Y.-F. *J. Am. Chem. Soc.* **2001**, *123*, 2791–2798.

(14) Dhara, S.; Datta, A.; Wu, C. T.; Lan, Z. H.; Chen, K. H.; Wang, Y. L.; Chen, L. C.; Hsu, C. W.; Lin, H. M.; Chen, C. C. *Appl. Phys. Lett.* **2003**, *82*, 451–453.

(15) Chang, C. Y.; Chi, G. C.; Wang, W. M.; Chen, L. C.; Chen, K. H.; Ren, F.; Pearton, S. J. *J. Electron. Mater.* **2006**, *35*, 738–748.

(16) Dhara, S.; Datta, A.; Wu, C. T.; Lan, Z. H.; Chen, K. H.; Wang, Y. L.; Chen, L. C.; Hsu, C. W.; Lin, H. M.; Chen, C. C. *Appl. Phys. Lett.* **2004**, *84*, 3486–3488.

(17) Dhara, S.; Datta, A.; Hsu, C. W.; Wu, C. T.; Shen, C. H.; Lan, Z. H.; Chen, K. H.; Chen, L. C.; Wang, Y. L.; Chen, C. C. *Appl. Phys. Lett.* **2004**, *84*, 5473–5475.

(18) Dhara, S.; Datta, A.; Wu, C. T.; Chen, K. H.; Wang, Y. L.; Muto, S.; Tanabe, T.; Hsu, C. W.; Shen, C. H.; Chen, L. C.; Maruyama, T. *Appl. Phys. Lett.* **2005**, *86*, 203119−1-3.

(19) Nam, C. Y.; Kim, J. Y.; Fischer, J. E. *Appl. Phys. Lett.* **2005**, *86*, 193112-1-3.

(20) Tham, D.; Nam, C. Y.; Fischer, J. E. *Adv. Mater.* **2006**, *18*, 290–294.

(21) Tao, L.; Khursheed, A. *IEEE Trans. Device Mater. Reliab.* **2006**, *6*, 182–185.

(22) Fang, C.; Wang, X.; Hu, G.; Xiao, H.; Wang, B.; Guo, L.; Li, J.; Li, C. 8th International Conference on Solid-State and Integrated Circuit Technology, Oct 23−26, 2006, Shanghai, China; IEEE Press: Piscataway, NJ, 2006; pp 902−904.

(23) Boguslawski, P.; Briggs, E.; Bemholc, J. *Phys. Rev. B* **1995**, *51*, 17255–17258.

(24) Neugebauer, J.; van de Walle, C. G. *Phys. Rev. B* **1994**, *50*, 8067–8070.

(25) Ginige, R.; Cherkaoui, K.; Wong Kwan, V.; Kelleher, C.; Corbett, B. *J. Appl. Phys.* **2004**, *95*, 2809–2815.

JP1020998